ELSEVIER

Available online at www.sciencedirect.com
SCIENCE DIRECT®

Nuclear Instruments and Methods in Physics Research A 541 (2005) 122–129

NUCLEAR INSTRUMENTS & METHODS IN PHYSICS RESEARCH
Section A

www.elsevier.com/locate/nima

Test of ATLAS SCT barrel modules with Nd:YAG laser

K. Hara[a,*], M. Minagawa[a], T. Kuwano[a], K. Nakamura[a], Y. Nakamura[a], H. Sengoku[a], Y. Ikegami[b], T. Kohriki[b], T. Kondo[b], S. Terada[b], Y. Unno[b], R. Takashima[c], I. Nakano[d], R. Tanaka[d], Y. Iwata[e], T. Ohsugi[e]

[a]*Graduate School of Pure and Applied Sciences, University of Tsukuba, 1-1-1 Ten'nodai, Tsukuba, Ibaraki 305-8571, Japan*
[b]*High Energy Accelerator Research Organization (KEK), Oho 1-1, Tsukuba, Ibaraki 305-0801, Japan*
[c]*Kyoto University of Education, Fukakusa-Fujimori, Kyoto 612-8522, Japan*
[d]*Department of Physical Science, Okayama University, 3-1-1 Tsushima-naka, Okayama 700-8530, Japan*
[e]*Department of Physical Science, Hiroshima University, 1-3-1 Kagamiyama, Higashi-Hiroshima 739-8526, Japan*

Available online 4 February 2005

Abstract

As a part of the quality assurance procedure of the ATLAS SCT (Semiconductor Tracker) barrel modules, the response of the microstrip detector is measured by injecting focused Nd:YAG laser at each strip. The test is sensitive to sensor originated problems and a cross check to the results obtained from the electrical tests performed with the test pulse system implemented in the readout ASICs. Combining these results with the probing results obtained by the silicon sensor manufacturer, we verified the reliabilities of these tests and classified the type of defects for overall performance evaluation of the modules.
© 2005 Published by Elsevier B.V.

PACS: 29.40.Gx; 29.40.Wk

Keywords: Silicon microstrip detector; ATLAS SCT; Laser test

1. Introduction

The ATLAS SCT (Semiconductor Tracker) group is constructing silicon microstrip detector modules [1] for the LHC Collider Experiment. The SCT modules are arranged into four concentric barrels in the central region and nine discs each in the forward/backward regions. All the barrel modules, in total 2112, are identical in design. Each module has four microstrip sensors, 63.56 mm × 63.96 mm, glued back-to-back on to a baseboard. The strips of the two sensors on the same side are wirebonded together. This effectively makes the strips 124 mm long with a pitch of 80 μm. A stereo angle of 40 mrad is subtended between the top and bottom strips.

*Corresponding author.
E-mail address: hara@hep.px.tsukuba.ac.jp (K. Hara).

0168-9002/$ - see front matter © 2005 Published by Elsevier B.V.
doi:10.1016/j.nima.2005.01.048

A flexible Cu-polyimide base hybrid [2], where 12 ABCD3T [3] binary readout ASICs are mounted, bridges over the module at the middle. With carbon–carbon backing, the hybrid is glued on extrusions of the baseboard without touching the sensor surface. The carbon–carbon backing and TPG (thermal pyrolytic graphite) baseboard efficiently draws the heat generated in ABCD3Ts and sensors (after radiation damage) toward one of the extrusions where a cooling pipe is coupled.

The barrel modules are constructed at four qualified construction sites. Although the module assembling systems are not identical among the sites [4], a thorough quality assurance is being carried out based on an agreed program. Together with sensor IV scans and thermal cycling tests, a common electrical test procedure is carried out using the test pulse system incorporated in the ABCD3T chips. This fully characterizes the functionality of the chip. The ABCD3T chip possesses 4-bit trim DACs to adjust channel-by-channel offsets. The chip gain, noise and offset are measured with and without the trim DAC adjustment. Channels with abnormal gain or offset may fail this adjustment. These channels can be masked in subsequent tests and during data taking. Another aspect of the measurements is determining the status of the wirebonding to the sensor strips. There are two categories which are unbonded and partially bonded that are determined from noise measurements. Small noise of the ABCD3T indicates either both strips, "unbonded", or one strip, "partbonded", are not "seen" at the input.

All the sensors for the barrel modules were fabricated by Hamamatsu Photonics (HPK), where extensive sensor probing was performed. The defects are categorized into Aℓ bridge, Aℓ break, implant bridge, implant break, and pinhole. The reliability of HPK probing had been checked at the prototyping and early production stages and was found to be acceptable.

The laser test described here has been performed on every module exclusively at the Japanese module production site. The purpose is to cross check the results obtained by the electrical test and sensor probing, and to provide an overall defect evaluation of the modules.

2. Laser test system and measurements

Since the energy of Nd:YAG laser 1.165 eV is just above the Si band gap energy of 1.12 eV, most of the laser light penetrates the Si sensor. Thus the passage of charged particles can be simulated if the laser is collimated and its intensity properly adjusted.

The laser test system consists of a set [5] of the laser head (Spectra-Physics Model S12-1060) with intensity controls and focusing lens, XY and Z stages, and an SCT-DAQ system based on VME [6].

The module under test is placed inside a module box for protection. It has slit windows for injection of the laser light. The module temperature is stabilized by placing the box on a water cooled (5 °C) Cu block which is fixed to the XY stage. The module is shifted horizontally by the XY-stage controlled through RS-232C with a feedback precision of 1 μm. The Z-stage is a GPIB controlled stepping motor (1.5 μm step) that regulates the vertical movement of the laser head and focusing microscope.

The whole system is triggered by a master pulser. On receiving a TTL-level signal, the laser power supply stops sending RF pulses to the Q switch in the laser head. The laser lights accumulated in the YAG rod are then liberated in a time duration of about 15 ns (6 ns FWHM). The laser intensity is adjusted through a polarizer and a set of neutral-density filters. The laser is focused on the sensor surface with a spot 2–3 μm square.

The master pulse is branched and fed to level one accept (L1A) of the SCT-DAQ system to initiate data acquisition. The response of a channel is evaluated by performing a threshold scan because of the binary readout scheme employed by the ABCD3T. Once the threshold scan is completed the module is shifted to the next strip so its evaluation can continue. Since two sensor strips are wirebonded to one ABCD3T channel, the scan is performed along two lines per side in order to be sensitive to sensor related problems such as Aℓ electrode breaks. The two scan lines (named Line-1 and Line-2) trace a path across the Aℓ strips at the far ends with respect to the readout ends.

Fig. 1 shows the response variation as a function of the laser injection point measured from the strip center. Also shown are dependences on Z. The XY position of the module is calibrated by locating two fiducial marks of one of the sensors. The precision of this measurement is typically 3 μm. This precision can be translated to 5 μm at the position along the scan lines. The thermal deformation could further degrade the precision. In order to avoid this the XY calibration is performed after the system has achieved thermal stability. This takes 5–10 min after the module is attached to the system. The nominal injection point is set at 25 μm from the strip center with the laser focused on the sensor surface. Concerning the Z control, although Z dependence is moderate, the module Z position is measured at three points along each of the two scan lines and parabola functions are used to interpolate Z at other strips. This is necessary because the module is not flat by about 50 μm due to warps of the sensors and the baseboard [4]. The Z calibration can be achieved better than 15 μm. From Fig. 1, the Z and XY precisions could introduce a module-to-module response variation of 7% at most.

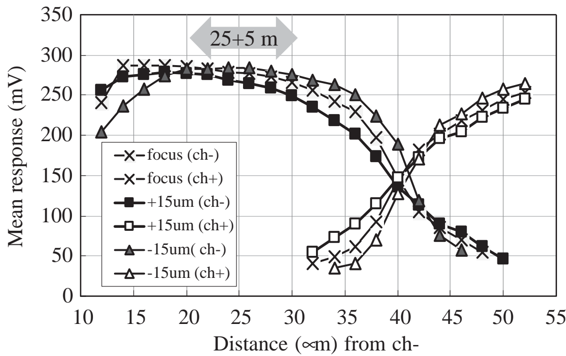

Fig. 1. Mean outputs (mV) of two neighboring strips as a function of the distance from the left strip. The curves are shown for the three cases where the laser spot is focused on the sensor surface (crosses), 15 μm upper (squares), and 15 μm lower. In the laser test, the spot is located nominally 25 ± 5 μm from the left when the response of the left strip is examined. The strip pitch is 80 μm.

The most important system performance is the time required to complete the scan while achieving precise measurements of the chip's gain and noise. The peak production rate of four modules a day introduced the constraint that on each module the test must complete in 2 h. This includes the time required to achieve thermal stability, the XY and Z calibrations and pedestal measurements. One parameter that can have a direct impact on the time taken to perform a scan is the master clock frequency. In Fig. 2 the output response and time required to complete a set of threshold scan are shown as a function of the master clock frequency. The laser output starts to decrease above 1 kHz, and SCT-DAQ system hangs above 2 kHz. From these curves, the master clock is set to 1 kHz.

The laser intensity is adjusted to about 300 mV at the ABCD3T threshold. Taking into account the pedestal of 20 mV on the average, this corresponds to the input charge of approximately 5 fC. The scan is composed of 10 threshold points and for each point 50 events are acquired. Under these conditions the measurement per strip takes 1.6 s with the threshold scan requiring 1.3 s and the stage movement and data validation taking 0.3 s. Hence a total of 40 min is required to complete one

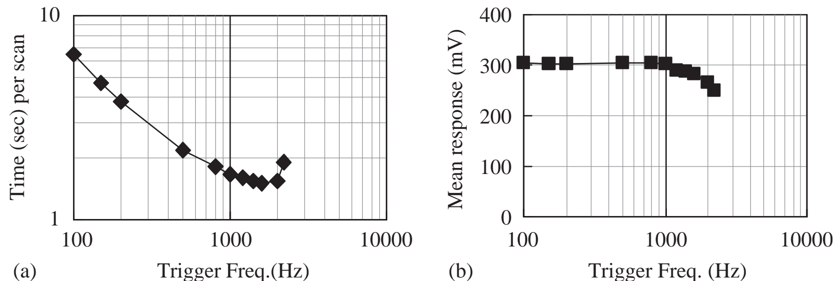

Fig. 2. (a) Time (s) to complete a threshold scan and (b) mean response (mV) as a function of the trigger frequency.

side of the module. The mean and sigma of the error function which is fitted to the threshold curve are the mean strip response and its spread. When picking up the 10 different threshold points there are two considerations. The first one is that at least two points are low enough but above the pedestal to study cross-talk between strips. The points 100 and 130 mV are chosen for this purpose. The second is that at least two points should be located in the transition region of the threshold curve in order to extract the mean and its spread with a reasonable precision. The nominal region is from 220 to 360 mV at a step of 20 mV. The region is shifted accordingly and the threshold curve is re-measured if the fitted mean is outside the nominal region. Also, in order to deal with the cases where some dust absorbs the laser, the same threshold scan is repeated at a shifted illumination point when the response is low.

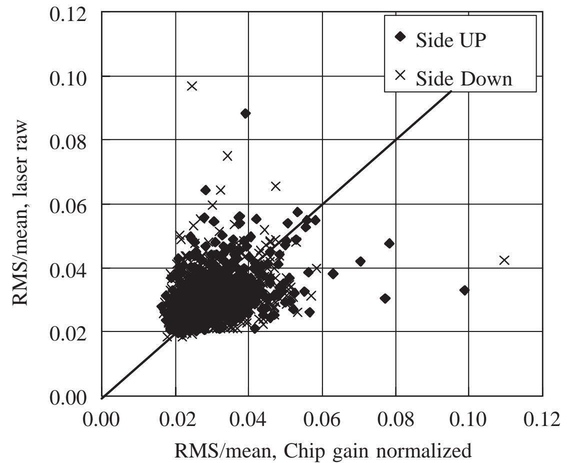

Fig. 3. Correlation between the relative RMS spread for laser raw response and that for the response normalized by the chip gain (see text).

3. Results

The module production is currently under way. The results to be shown are gathered from a total of 656 modules.

3.1. Response mean and spread

The laser response is 271 mV on the average after pedestals are subtracted. This is about 5.12 fC at the input charge by taking account of the mean ABCD3T gain of 52.9 mV/fC. The RMS spread of the mean is 7.7%, representing the sum of contributions of the ABCD3T gain variation (4.6%), response variation due to incomplete XY and Z calibrations ($<7\%$), and laser intensity variation. Among these, the contribution of the laser intensity variation is largest. The same system was used for other study where the laser intensity and spot size were varied and no effort was made to set precisely the conditions back. Instead the relative spread, defined as the RMS spread divided by the mean, was evaluated for each side of the module. Fig. 3 plots the correlation between the relative spread calculated from the raw response and from the response which is corrected for different ABCD3T gain per channel basis. The average of the relative spread is 3.07% (RMS variation is 0.75%) for raw response and 3.00% (RMS variation is 0.84%) for the gain corrected response.

In the plot, the data points located upper left are characteristic where the large raw response variation is explained by the large ABCD3T gain spread. On the other hand, those located lower right are worse if corrected by the ABCD3T gains. This could be explained partially by wrong evaluation of the calibration capacitors of the chip. This is one of the purposes of the laser test which can provide direct and independent evaluations of the chip gains. In fact it turned out that one chip of the module at the extreme point is taken from a wrong chip production batch where the calibration capacitors are quite different. Many of the points, though, are for irregular modules [6] and larger variation of gain corrected response can be explained by the temperature difference between the laser and electrical tests. The ABCD3T chips of such modules are found to be sensitive to the operation conditions such as the strobe timing and shaper current, both being dependent on the temperature. Nevertheless, it can be noted that 98.4% of the module sides have the gain spread smaller than 5% without the chip gain correction.

3.2. Defective channels

The number of defective channels per module is histogrammed in Fig. 4, where the data are given with and without including marginal noisy channels (see below). Modules are classified as good if it possesses less than 15 (1%) defective channels. Only one out of the 656 tested modules failed.

The defective channels are categorized by combining all the information, HPK probing result, electrical test result, laser test result and visual inspection. A summary is given in Table 1. For 656 modules, the number of defective channels judged by the electrical test is 774 including noisy channels. Although the laser test is not precise enough to perform detailed comparison of the noisy channels because of limited threshold step size and number of events, it can detect noisy channels if the noise exceeds typically 50% larger than the normal. The total number 477 in the table excludes most of the noisy channels but includes 28 very high noise channels identified also by the laser test. Of 477 defects, about a half are due to incomplete wirebonding. We did not try to re-wirebond, when wirebonding failed, for a certain period of the production, since it was thought to increase the detector leakage current. After the decision that we re-wirebond but only once, the defect fraction decreased. About a quarter are due to the sensor related problems, and $\frac{1}{5}$ are the ABCD3T chip related problems. The detailed breakdown of the chip problem can be found elsewhere [6]. The defects of the pitch adaptors are three breaks and one short. This only one short is created by a droplet of silver epoxy glue. There existed in addition six pairs of bridges, which are not shown in the table. These bridges were trimmed off by the same laser system but set at higher intensity. There are three channels identified to be defective by the laser but judged normal by the electrical test. Repeated measurements provided consistent disagreement. Although a part of the sensor surface is covered by the hybrid, visual inspections could not find any trace of defects.

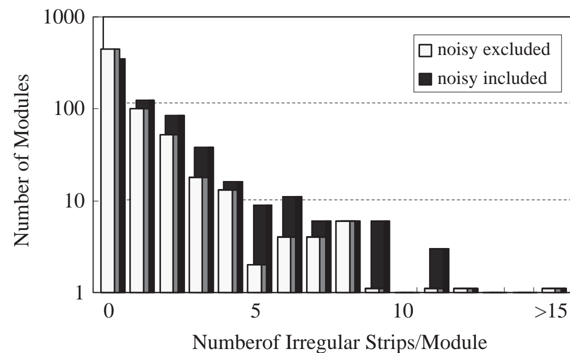

Fig. 4. Number of defective channels per module for a total of 656 modules. The open (filled) histogram is with noisy channels excluded (included).

Table 1
Summary of the defective channels for 656 modules

Number of modules tested	656	
Number of channels tested	1,007,616	100%
Defective channels (excl. noisy)	477	0.047%
(A) Sensor defects	116	(0.012%)
$A\ell$ bridge	(87)	
$A\ell$ break	(22)	
Implant break	(7)	
(B) ABCD3T chip defects	93	(0.009%)
dead/digital problem	(30)	
gain or offset problem	(63)	
(C) Pitch adaptor defects	5	(0.001%)
(D) Incomplete wirebonding	232	(0.023%)
(E) Very high noise	28	(0.003%)
(F) Reason not identified	3	(0.000%)

The number of defective channels (excluding 318 marginal noisy channels) was 477. Their defects are arranged into categories (A)–(F). The numbers listed below (A) and (B) are their breakdowns.

3.3. Consistency with HPK probing

The comparison between the HPK probing and laser results is summarized in Table 2. The HPK probing judged 620 sensor strips to be defective.

Among the 85 $A\ell$ bridges, 81 are identified by laser. For the remaining two pairs, a remnant of bridge is recognized by visual inspection. It seems that the pairs were in contact originally but the bridge should have brown off when the neighboring strip was probed. We found six new bridges,

two 3-strip bridges. These are known by HPK probing but have been judged as pinholes. There is a tendency that HPK judges bridges as pinholes if more than two strips are connected.

Among the 31 $A\ell$ breaks, we identified 19 and the rest turned out to be normal. In addition, we identified three new breaks which were not seen by HPK. Photographs of the three defects and another one (described later) are shown in Fig. 5. Since a trace of discharge is visible in (a), the strip may have broken by discharge initiated at the neighboring strip which was probed after the "later broken" strip. The passivation in (b) is damaged, which may have disturbed the HPK probing judgement. The break of (c) is clear and needs to be explained why this was not identified by HPK.

Table 2
Comparison with HPK probing results

Number of strips	2,015,232		
	HPK	ID'ed	New
$A\ell$ bridge	85	81 + 4	+ 6
$A\ell$ break	31	19	+ 3
Implant bridge	0	0	+ 0
Implant break	8	(7)	—
Pinhole	496	—	—

The numbers in Column "ID'ed" are the defects identified by our tests out of the numbers in Column HPK. The column "new" lists the numbers which are not detected by HPK. The numbers in parentheses are from visual inspections, and those with—are not detectable by our tests.

The silicon sensors with implant breaks are assembled into modules with the bias resistors placed far side to the readout. Under this arrangement, the implant electrode where the laser is injected would be biased normally and detecting the implant break is inefficient because the signal would be picked up normally to the $A\ell$ electrode. Instead, we investigated the implant breaks under a microscope. Out of 8 implant breaks, 7 are identified and 1 is normal.

The pinholes cannot be detected both by the electrical and laser tests. Summarizing the HPK probing reliability, only one $A\ell$ break out of 9 new defects should be attributed as a thorough mistake, while the HPK probing provides somewhat over-estimated evaluation of defective channels especially for $A\ell$ breaks.

3.4. Consistency with electrical testing

Table 3 summarizes the comparison between the electrical and laser tests.

There are 23 defective channels which are identified by laser but not by electrical test. Among these, 16 are the $A\ell$ breaks which have been identified also by HPK. Of 4 defects which are detected by the laser test only, 3 are new $A\ell$ breaks

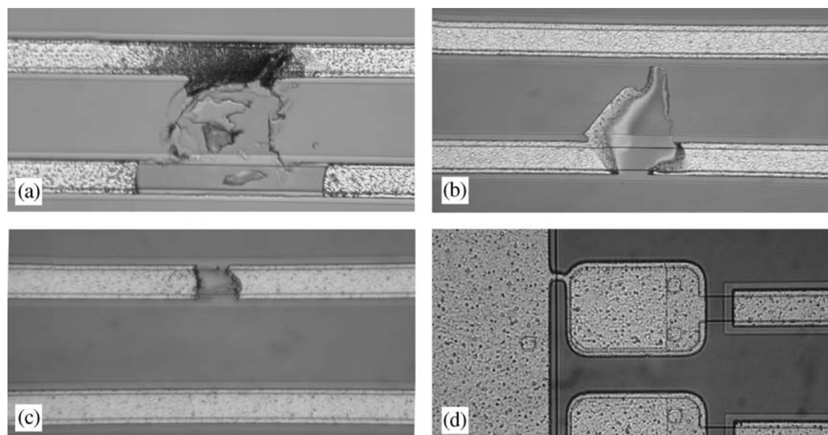

Fig. 5. (a)–(b) $A\ell$ breaks and (d) a bridge between DC pad and bias-ring. These were not identified by HPK probing.

Table 3
Comparison with electrical test results. The numbers in parentheses are breakdowns

Number of channels	1,007,616	
Defects not detected by electrical test	23	
Aℓ breaks identified by laser and HPK		(16)
New sensor defects identified by laser only		(4)
New defects, but reason not identified		(3)
Judgement error by electrical test	10	
Trim error		(7)
Wire-bonding judge mistake		(3)
Irregular (>15% off the average) but usable	94	

listed in Table 2, and 1 is a bridge found between the DC pad and bias-ring (see Fig. 5d). The three "new defects, but reason not identified" are those channels listed as (F) in Table 1. Of 116 sensor defects, listed as (A) in Table 1, the electrical test missed to detect 20 channels.

There are 10 channels which are to be attributed to the errors of the electrical test judgement. Seven are the errors in the trim DAC adjustment of ABCD3T chips probably due to pick-up noise during the calibration measurements: these were re-tested and found to be normal. The three "wire-bonding judge mistakes" are due to that the measured noise levels are just around the judgement boundary.

The laser test found 94 channels which have a response off the local average by more than 15% but are qualified to be usable by electrical test. Note that the laser test is performed without trim DAC adjustment. These channels turned out to have negative pedestals but are within the range ($> -100\,\mathrm{mV}$) recoverable by the trim DAC adjustment.

Summarizing the above, 7 trim errors could be attributed to the real mistakes of the electrical test out of 2 million channels examined, since the electrical test is expected not to be sensitive to detect sensor originated problems (20 and probably 3 more) and wire-bonding judge mistakes (3) could be recovered by algorithm tuning.

4. Summary

A total of 656 ATLAS SCT barrel modules are tested by injecting focused Nd:YAG laser at each strip. The test is sensitive to the sensor originated problems and a cross check to the HPK probing results and calibration results obtained by the electrical test. All the above information and visual inspections are gathered to evaluate the reliability of the HPK probing and electrical tests.

The overall defective channel fraction is 0.047% on the average without including marginal noisy channels. Incomplete wirebonding, sensor defects, and ASIC chip defects are the main causes. The HPK probing provided in general reliable but somewhat over-estimated evaluation of the Aℓ strip breaks. Only one Aℓ break was missed to detect out of over 2 million strips probed. The electrical test missed to detect 20 sensor defects out of in total of 116 defects, and resulted 7 wrong trim DAC calibrations out of over 1 million ASIC channels.

Acknowledgements

We would like to acknowledge the many people involved in the SCT module design and production, and also who have developed the SCT-DAQ system. Especially we would like to thank G. Moorhead for providing us the software for the SCT data acquisition. S. Inaba and M. Yokoshima are also to be acknowledged for their continuous help in the module measurement.

References

[1] K. Kondo, et al., Nucl. Instr. and Meth. A 485 (2002) 47.
[2] Y. Unno, et al., Nucl. Instr. and Meth. A, this issue doi:10.1016/j.nima.2005.01.068;
Y. Unno, Proceedings of Sixth Workshop on Electronics for LHC Experiments, CERN/LHCC/2000-41, p. 66.
[3] W. Dabrowski, et al., Proceedings of the Fourth Workshop on Electronics for LHC Experiments, CERN/LHCC/98-36, p.175;
W. Dabrowski, et al., Proceedings of the Fifth Workshop on Electronics for LHC Experiments, CERN/LHCC/99-33, p.113;

W. Dabrowski, et al., Proceedings of the Sixth Workshop on Electronics for LHC Experiments, CERN/LHCC/2000-41, p. 115.
[4] Y. Kato, et al., Nucl. Instr. and Meth. A 511 (2003) 132; Y. Ikegami, et al., Proceedings of the Eighth Workshop on Electronics for LHC Experiments, CERN/LHCC/2002-23, p. 116.
[5] Y. Unno, et al., Nucl. Instr. and Meth. A 383 (1996) 238.
[6] D. Robinson, Nucl. Instr. and Meth. A 485 (2003) 84; A. Ciocio, Nucl. Instr. and Meth. A, this issue.